Environmental Science & Technology

Article

Cite This: Environ. Sci. Technol. 2019, 53, 8664−8671

pubs.acs.org/est

Estimating Secondary Organic Aerosol Production from Toluene Photochemistry in a Megacity of China

Yaqin Gao,[†,‡] Hongli Wang,*[,†] Xuan Zhang,[§] Sheng'ao Jing,[†] Yarong Peng,[†,‡] Liping Qiao,[†] Min Zhou,[†] Dan Dan Huang,[†] Qian Wang,[†] Xiang Li,*[,†,‡] Li Li,[†] Jialiang Feng,[∥] Yingge Ma,[†] and Yingjie Li[†]

[†]State Environmental Protection Key Laboratory of Formation and Prevention of the Urban Air Pollution Complex, Shanghai Academy of Environmental Sciences, Shanghai 200233, China

[‡]Department of Environment Science and Engineering, Fudan University, Shanghai 200433, China

[§]Atmospheric Chemistry Observation & Modeling Laboratory (ACOM), National Center for Atmospheric Research (NCAR), Boulder, Colorado 80301, United States

[∥]School of Environmental and Chemical Engineering, Shanghai University, Shanghai 200444, China

Supporting Information

ABSTRACT: The production of secondary organic aerosols (SOA) from toluene photochemistry in Shanghai, a megacity of China, was estimated by two approaches, the parametrization method and the tracer-based method. The temporal profiles of toluene, together with other fifty-six volatile organic compounds (VOCs), were characterized. Combing with the vapor wall loss corrected SOA yields derived from chamber experiments, the estimated toluene SOA by the parametrization method as embodied in the two-product model contributes up to ∼40% of the total SOA budget during summertime. 2,3-Dihydroxy-4-oxopentanoic acid (DHOPA), a unique product from the OH-initiated oxidation of toluene in the presence of elevated NO_x, was used as a tracer to back calculate the toluene SOA concentrations. By taking account for the effect of gas-particle partitioning processes on the fraction of DHOPA in the particle phase, the estimated toluene SOA concentrations agree within ∼33% with the estimates by the parametrization method. The agreement between these two independent approaches highlight the need to update current model frameworks with recent laboratory advances for a more accurate representation of SOA formation in regions with substantial anthropogenic emissions.

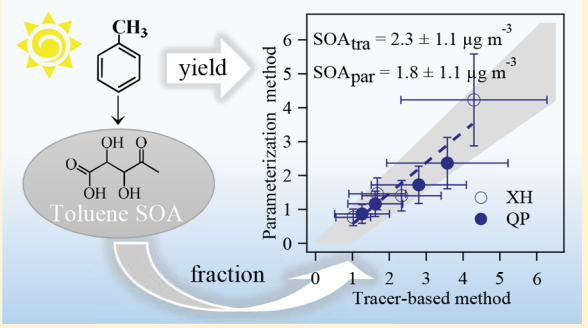

1. INTRODUCTION

Secondary organic aerosol (SOA) constitutes a major fraction (20−80%) of particulate organic matter (OM) in the ambient atmosphere, and it profoundly influences air quality, climate change, and human health.[1−3] Anthropogenic aromatics, a significant fraction of volatile organic compounds in the urban atmosphere, have been suggested as an important SOA precursor.[4−9] The contributions of aromatics derived SOA to the overall SOA budget in different urban areas have been estimated mainly through two approaches, that is, the two-product model and the tracer-based method. The two-product model is an empirical gas−particle partitioning model optimized to chamber SOA yield data. The best-fit parameters are further incorporated in 3-D transport models for the predictions of SOA formation from a given hydrocarbon system in the atmosphere. Using this method, studies have estimated that the removal of aromatic precursors under low-NO_x conditions accounted for approximately ∼37% of the secondary formation in the United States,[7] whereas under high-NO_x conditions, significantly less SOA formation is attributed to aromatics photochemistry, for example, ∼11% at Paris[10] and 10.6−13.9% at Changdao, China.[8] The tracer-based method is widely used for SOA source appointment.[6,11,12] In principle, an oxidation product that is unique to a given hydrocarbon system can serve as a tracer for the estimation of the ambient SOA produced from this particular hydrocarbon based on the tracer-to-SOA ratio that is measured in chamber experiments. With this method, field studies have estimated that toluene contributes ∼15−79% to the overall identified SOA in megacities in China, including Beijing, Shanghai, Guangzhou, and Hong Kong.[4−6,11,13−15]

Compelling evidence from field observations suggests that current SOA models consistently underpredict the ambient organic aerosol concentration.[16−19] Such underprediction is likely a result of a number of factors. The traditional SOA

Received: January 30, 2019
Revised: June 27, 2019
Accepted: July 2, 2019
Published: July 2, 2019

DOI: 10.1021/acs.est.9b00651
Environ. Sci. Technol. 2019, 53, 8664−8671

models constrained by chamber experiments do not account explicitly for atmospheric aging. Further, the VOC emission inventories that drive atmospheric models in all likelihood understate the fluxes of key SOA precursors,[20] and the addition of more complete SOA precursor inventories into models has not yet satisfactorily resolved the gap between measurements and predictions.[21] Most recently, chamber experiments have demonstrated that vapor losses can lead to substantial underestimations in SOA formation,and accounting for such losses could have the potential to bring model and measurement into closer agreement.[22]

Shanghai, the biggest city in China, is facing serious air pollution due to rapid urbanization and industrialization, arousing people's great concern about visibility reduction and public health impact. The annual average $PM_{2.5}$ showed a decrease trend (from 101.7 to ∼60 $\mu g\ m^{-3}$) from 1999 to 2012.[23] In response to the severe haze event of 2013, the Chinese State Council released the "Atmospheric Pollution Prevention and Control Action Plan" in September 2013.[24] Since then, The concentration of $PM_{2.5}$ decreased from 79 to 32 $\mu g\ m^{-3}$ as of 2017.[25] However, the relative contribution of secondary fraction to $PM_{2.5}$ has been increasing compared to the primary fraction. In particular, the relative contribution of secondary organic carbon (SOC) to organic carbon (OC) showed an increasing trend from 20%[26] in 2013 to 52.2% in 2017.[27−29] Recent studies in Shanghai have shown that OM contributed to 48% of the PM mass, and SOA accounted to 44−71% of organic aerosols.[26,28] Similarly, the long-term trends of O_3 from 2006 to 2015 in Shanghai increased by 67%[30], suggesting that secondary pollution has become a serious air quality problem in Shanghai.

In this study, we employ the parametrization method as embodied in the two-product model and tracer-based method to estimate the SOA production from toluene photochemistry during a pollution episode of the summer 2014 in a megacity of China, Shanghai. We account for the vapor wall loss processes in the parametrization of chamber-derived SOA yields from toluene as well as a series of other VOCs. We update the tracer-based method by considering the gas−particle partitioning and the photochemical processes that lead to the toluene tracer formation. The surface level of the toluene derived SOA at two observational sites that are representative of the urban and suburban area of Shanghai was evaluated by comparing the outputs of the two approaches.

2. EXPERIMENTAL SECTION

2.1. Sampling and Analysis. Field measurements were carried out during a photochemical pollution episode from 4 to 7 August in summer 2014 at two ground sites that are representative of Shanghai urban area (site XH, 31.170° N, 121.431° E, 15 m above ground level) and suburban area (site QP, 31.136° N, 121.092° E, 10 m above ground level), see the map in Supporting Information (SI) Figure S1. Site XH is located in the city center, surrounded by residential buildings and under strong influence of vehicle emissions. Site QP is located northwest of the city center ∼32 km from the XH site. The landscape surrounding the QP site is a mix of polluted air masses by regional transport and local biogenic emissions. During the campaign, O_3, NO, NO_2, and meteorological parameters were constantly monitored.

VOCs samples were collected using SUMMA canisters (Entech Instruments, Simi Valley, CA) five times per day at 09:00 (07:30−10:30), 12:00 (10:30−13:30), 15:00 (13:30−16:30), 18:00 (16:30−19:30), and 21:00 (19:30−7:30 + 1 day), and then analyzed off-line by a custom-built two-channel gas chromatography coupled with a mass spectrometer and a flame ionization detector (GC-MS/FID).[8] The FID channel with a PLOT Al_2O_3 capillary column (15 m × 0.32 mm × 3.0 μm, J&W Scientific, Folsom, CA) is used to measure C_2-C_5 hydrocarbons and the MS channel with a DB-624 capillary column (30 m × 0.25 mm × 1.4 μm, J&W Scientific) is targeted for other species. Calibration was conducted by PAMS standards (Spectra Gases Inc., Stewartsville, NJ) with a concentration range of 0−8 ppbv. A total of 57 nonmethane hydrocarbon species, including alkanes, alkenes, and aromatics, were measured, with detection limits in the range of 0.002−0.121 ppbv.

$PM_{2.5}$ samples were collected on quartz filters (20.3 cm × 25.4 cm, Whatman QM-A, U.K.) during daytime (07:30−19:30) and nighttime (19:30−07:30 + 1 day) using high volume samplers operated at 30 $m^3\ h^{-1}$. Each quartz filter was divided to two parts for SOA speciation and total carbon analysis. The filter handling and extraction protocols for SOA speciation have been described previously.[14] Briefly, the filter with spiked methyl-β-D-xylopyanoside (MXP) as the internal standard was ultrasonically extracted with 20 mL of dichloromethane and methanol (1:1, v/v) mixture at room temperature. The extracts were further dried by a gentle stream of ultrapure nitrogen and then derivatized with 100 μL N,O-bis(trimethylsilyl)-trifluoroacetamide (BSTFA, with 1% trimethylchlorosilane as catalyst) and 20 μL pyridine at 75 °C for 45 min. The resulting derivatives were analyzed by GC-MS (6890 GC/5975 MSD, Agilent Technologies Inc., Santa Clara, CA). The GC temperature was programmed to rise from 70 °C (held for 2 min) to 300 °C at 5 °C min^{-1} with a hold of 5 min. Ultrahigh-purity helium was applied as carrier gas with a flow rate of 1.0 mL min^{-1}. The MS was operated in the electron ionization mode at electron energy of 70 eV. Selected ion monitoring mode was used for the quantification of the target SOA tracers: m/z 204 and 217 for MXP and m/z 247 for 2,3-dihydroxy-4-oxopentanoic acid. SOA tracers were quantified using MXP as the surrogate as MXP is not found in atmospheric samples and its derivatives features a distinctive mass spectrum.[12,14] Toluene SOA tracer 2,3-dihydroxy-4-oxopentanoic acid was identified. The remaining quartz filter was used for the elemental carbon (EC) and OC analysis with a thermal/optical carbon analyzer (DRI 2001A, Atmoslytic Inc., Calabasas, CA).

Field and laboratory blanks were extracted and analyzed in the same manner. The target compounds were not detected in the blank samples. The extraction efficiency was evaluated by adding MXP to each filter sample half hour earlier prior to extraction. The recovery was 70−110% for MXP, suggesting that the extraction efficiency of the SOA tracers is acceptable. The measured differences in the concentrations of target compounds in paired duplicate samples were less than 20%.

2.2. Total SOA Estimation by the EC-Tracer Method. The total SOA concentration was estimated using the EC-tracer method (SOA_{EC}), which has been widely used in previous studies:[31−33]

$$SOA = SOC \times 1.8 \quad (1)$$

$$SOC = OC - EC \times \left(\frac{OC}{EC}\right)_{pri} \quad (2)$$

DOI: 10.1021/acs.est.9b00651
Environ. Sci. Technol. 2019, 53, 8664−8671

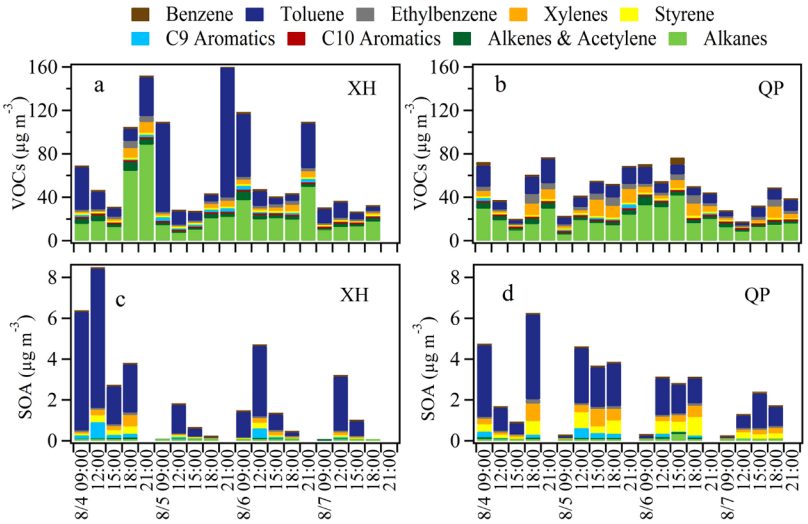

Figure 1. Concentrations of measured VOC precursors and SOA estimated by the parametrization method at the urban (XH) and suburban (QP) sites in Shanghai.

where the SOA to the SOC ratio in summertime Shanghai was estimated as 1.8,[34] and the OC to EC ratio for primary emissions $(OC/EC)_{pri}$ (1.32 at XH and 1.36 at QP) was estimated using the observed minimum OC/EC ratio.[35,36] These estimated values are comparable with those (1.8 at XH and 1.6 at QP) derived via linear regression of the 20th percentile of the entire measurements.[37]

2.3. SOA Estimation by Parametrization Method. The parametrization method is used to estimate the SOA production from a given VOC:[38,39]

$$SOA_{par} = VOC_{i,consumed} \times Y_i \quad (3)$$

where Y_i, the SOA yield from a given VOC_i, is calculated as the mass ratio of the SOA produced to the parent hydrocarbon reacted. Here, alkanes and aromatics with more than six carbons are considered as potential SOA contributors in our calculation.[8,40] Other potential precursors such as intermediate VOCs (IVOCs) and semi-VOCs (SVOCs) were not included in this study due to our measurement limitations. SOA yields measured under high-NO_x conditions from previous chamber studies (as shown in SI Table S1) are scaled to the ambient conditions ([OA] = 15.0 μg m^{-3}, T = 304 K) during the sampling period and further corrected for vapor wall losses.[22] $VOC_{i,\ consumed}$, the amount of VOC_i oxidized by the OH radical, is calculated based on the photochemical age via eq 4):

$$VOC_{i,consumed} = VOC_{i,t} \times (\exp(k_i[OH]\Delta t) - 1) \quad (4)$$

where *the OH exposure*, $[OH]\Delta t$, is the product of OH radical concentration [OH] and photochemical age Δt, given by[41]

$$[OH]\Delta t = \frac{1}{k_E - k_X} \times \left(\ln\frac{[E]}{[X]}\bigg|_{t=t_0} - \ln\frac{[E]}{[X]}\bigg|_{t=t} \right) \quad (5)$$

where k_E and k_X are the reaction rate coefficients for the OH oxidation of ethylbenzene (7.0×10^{-12} cm^3 molecule^{-1} s^{-1}) and m+p-xylene (18.9×10^{-12} cm^3 molecule^{-1} s^{-1}), respectively. $\frac{[E]}{[X]}\Big|_{t=t}$ is the measured ratio of ethylbenzene to xylene at time t. The temporal profiles of $\frac{[E]}{[X]}\Big|_{t=t}$, are shown in SI Figure S2. $\frac{[E]}{[X]}\Big|_{t=t_0}$ is the emission ratio of ethylbenzene to m+p-xylene assumed to be constant during the investigation period. This value was estimated as the ratio observed in the least processed air masses at night (SI Figure S2). The ratio of ethylbenzene to m+p-xylene is commonly used as an indicator for photochemical reactions because these chemicals are usually from common sources, and the reaction rate constant of m/p-xylene with the OH radical is approximately three times greater than that of ethylbenzene.[8,42−44] The OH exposure is a linear function of the logarithm of the measured ratio between the two hydrocarbons and equals to zero when the measured ratio is equal to the emission ratio.[45] This method has been applied in the Los Angeles,[38,45,46] Paris[47] and many other places of China.[8,48,49]

2.4. Tracer-Based SOA Estimation Method. The tracer-based method, as introduced by Kleindienst et al. (2007), has been widely used for the estimation of the contribution of individual biogenic and anthropogenic hydrocarbons to the SOA production via atmospheric photooxidation processes:[12]

$$SOA = \frac{[tr_i]}{f_{i,SOA}} \quad (6)$$

where $[tr_i]$ is the particle-phase concentration of tracer i (μg m^{-3}) in the ambient air, [SOA] is the to-be-determined concentration of SOA (μg m^{-3}) produced from the oxidation of a given hydrocarbon precursor in the ambient air, and $f_{i,SOA}$ is the fraction of the tracer i in the SOA produced from the same hydrocarbon precursor in chamber experiments. The premise behind the tracer-based method is that $f_{i,SOA}$ derived from chamber experiments remains constant in the ambient, although many environmental factors, such as temperature, free radical levels, total organic aerosol mass loading, etc., could modulate the pathway by which the tracer is formed in the particle phase and thereby affecting the value of $f_{i,SOA}$. Here we correct $f_{i,SOA}$ by accounting for the gas-particle partitioning processes, as discussed shortly.

2.5. Trajectory Cluster Analysis. Twenty-four-hour backward air trajectories arriving at the sampling location were calculated based on Hybrid Single-Particle Lagrangian Integrated Trajectory model (HYSPLIT 4.0) developed by Air

DOI: 10.1021/acs.est.9b00651
Environ. Sci. Technol. 2019, 53, 8664−8671

Resources Laboratory from National Oceanic and Atmospheric Administration (NOAA)[50] (http://www.arl.noaa.gov/ready/hysplit4.html). The model was run every 1 h, and the starting height was set at 200 m. A clustering technique, embedded in the free software TrajStat (http://www.meteothinker.com/TrajStatProduct.aspx), is performed to discriminate different transport trends/tendencies in the horizontal and vertical directions. Similar trajectories are paired to form clusters in the clustering analysis, from which maximized differences are found. More details of the clustering technique can be found in the references of the HYSPLIT model.[50]

3. RESULTS AND DISCUSSION

Continuous high temperature, low relative humidity, and strong solar radiation that favor photochemical pollution were observed during the campaign, see SI Figure S3. The 8-h average daytime concentrations of O_3, NO, NO_2 are 34.4 ± 23.3 ppb, 4.3 ± 2.3 ppb, and 14.8 ± 3.9 ppb, respectively, at Site XH and 46.0 ± 26.9 ppb, 2.5 ± 0.9 ppb, and 12.2 ± 2.7 ppb, respectively, at Site QP. The observed peak O_3 concentrations at the suburban site (131.1 ppb) are generally 13.6% higher than those at the urban site (115.4 ppb), owing to the limited NO titration and enhanced VOC oxidation (the diurnal OH exposure levels vary from 1.5×10^{10} molecules cm^{-3} to 4.5×10^{10} molecules cm^{-3} s at Site XH and from 1.21×10^{10} molecules cm^{-3} to 4.6×10^{10} molecules cm^{-3} s at Site QP). The daytime SOA concentrations estimated by the EC-tracer method (SOA_{EC}) account for 47.6% and 42.3% with range from 45.3%−52.0% and 29.8%−47.2%, respectively, of the total organic matter for Site XH and Site QP (SI Table S2 and Figure S4), and are positively correlated (R^2 = 0.81) with the O_3 average daytime concentration for both sites (SI Figure S5). These values are consistent with previous observations, for example, the average contribution of SOA to the total OM mass was 41.0% in Pearl River Delta[5] and 33.8% in Beijing.[51]

3.1. Toluene SOA Estimation by the Parametrization Method. Fifty-seven VOCs, classified as alkanes, alkenes, acetylene, and C_6−C_{10} single-ring aromatics, were detected, with total concentrations of 65.8 ± 43.8 μg m^{-3} at Site XH and 48.3 ± 18.5 μg m^{-3} at Site QP (Figure 1). Aromatics and alkanes dominate the overall VOC emission for both sites. The clustering analysis of 24 h air mass backward trajectories (SI Figure S6) computed by the NOAA HYSPLIT model[50] suggests that the trajectories primarily originated from the Pacific ocean with clean air masses, implying that the observed VOCs at Shanghai are primarily from local emissions. *Accordingly, the daily fraction of each VOC category is a result of local variations in emissions and photochemical processes* (SI Figure S7). Toluene is the most abundant anthropogenic VOC (26.3 μg m^{-3} at XH and 10.1 μg m^{-3} at QP), accounting for 40.0% and 21.0%, respectively, of the total VOC mass. The prevalence of toluene in Shanghai's air is consistent with earlier observations in other megacities of China, where high-aromatic fuels and solvent use are the predominant anthropogenic source.[52−55] Additionally, the OH reactivity of toluene is relatively low compared to the other nonparaffinic hydrocarbons, further extending its lifetime in the atmosphere.[56] A distinctive diurnal pattern of the VOC emissions was observed at Site XH, peaking at night (19:30−7:30 + 1d) followed by early morning (7:30−9:30). The observed peak VOCs concentration at the urban site (160.1 μg m^{-3}) is approximately twice as much as that at the suburban site (76.8 μg m^{-3}).

Also given in Figure 1 are the estimated SOA concentration profiles from photooxidation of the identified 57 VOCs by the parametrization method. The average SOA concentrations are 2.2 ± 2.4 μg m^{-3} and 2.5 ± 1.7 μg m^{-3}, respectively, and explain 29.3% and 37.3%, respectively, of the total SOA mass estimated by the EC-tracer method (SOA_{EC}) at Site XH and Site QP. The remaining unaccounted SOA mass is likely produced from the missing IVOCs and SVOCs, as well as the potential missing chemical production pathways such as ozonolysis of alkenes. The toluene SOA concentrations estimated by the parametrization method are 1.8 ± 0.7 μg m^{-3} and 1.5 ± 1.1 μg m^{-3}, respectively, contributing 23.6% and 22.8%, respectively, to the daytime SOA at Site XH and Site QP (see SI Table S3 for more details). While the toluene and NO_x levels at Site QP were much lower than those measured at Site XH, the photochemical losses of toluene and resulting SOA mass were actually comparable between the two sites due to different extents of OH exposure. The diurnal profile of toluene SOA, as shown in SI Figure S8, exhibits a noon peak maximum at XH, with featured concentration of 3.6 ± 2.0 μg m^{-3}. On the contrary, a continuous increase in the early afternoon was observed at Site QP, consistent with the estimated higher OH exposure in the suburban area.

3.2. Toluene SOA Estimation by the Tracer-Based Method. 2,3-Dihydroxy-4-oxopentanoic acid (DHOPA), a unique product from the OH-initiated oxidation of toluene in the presence of elevated NO_x, has been identified as a tracer for toluene SOA.[12] During the investigation period, the average daytime mass concentrations of DHOPA are 2.1 ± 2.1 ng m^{-3} at Site XH and 1.9 ± 1.4 ng m^{-3} at Site QP. These levels are comparable with previous measurements during the summer time in Shanghai (1.9 ± 1.7 ng m^{-3}), China,[14] Hongkong, China (∼1.6 ng m^{-3}),[13] Bondville, IL (1.8 ng m^{-3}),[57] and Iowa City, IA (∼0.3 ng m^{-3}),[58] but lower by approximately an order of magnitude compared with those reported in the Pearl River Delta region, China (15.1 ng m^{-3}),[5] Beijing, China (9.7−11.0 ng m^{-3}),[11] Riverside, CA (∼12.8 ng m^{-3}),[59] and Mexico City, Mexico (∼14.7 ng m^{-3}).[60]

Kleindienst et al. (2007) measured the fraction of DHOPA in the chamber derived toluene SOA under high-NO_x conditions as 0.0040 ± 0.0013. This value, although has been commonly applied for the estimation of toluene SOA in the ambient air, is subject to major uncertainties associated with environmental factors that could impact the gas-phase formation pathways and gas-particle partitioning of DHOPA. The average NO level during the field campaign is 2.5 ± 2.8 ppb (>1 ppb), and the ratio of VOCs to NO_x (VOCs/NO_x, ppbC/ppb) is 7.7 ± 4.4 (<10). Under such conditions, RO_2 radicals predominantly react with NO, consistent with the chemistry occurring under high NO_x conditions created in chamber studies. It is therefore reasonable to assume that the chemical pathways leading to DHOPA in chamber experiments are representative of the DHOPA production chemistry in the ambient air in Shanghai. To account for the effect of gas-particle partitioning on the observed mass fraction of DHOPA in the particle phase, we apply a five-bin Volatility Basis Set[61] to represent the observed toluene SOA masses in Kleindienst et al. (2007):

$$\text{toluene} + \text{OH}\cdot \rightarrow \alpha\cdot\text{tracer} \quad (7)$$

$$\text{toluene} + \text{OH}\cdot \rightarrow \sum_{i=1}^{5} \beta_i \cdot P_i \quad (8)$$

DOI: 10.1021/acs.est.9b00651
Environ. Sci. Technol. 2019, 53, 8664−8671

where α is the mass-based stoichiometric yield of the tracer and β_i is the mass yield of volatility bin P_i and its value is given in SI Table S4. The fraction of the tracer in the particle phase (f_{SOA}) is thereby expressed as

$$f_{SOA} = \frac{\Delta tol \cdot \alpha \cdot F_{pt}}{\Delta tol \cdot \sum_{i=1}^{5} \beta_i \cdot F_{Pi}} \quad (9)$$

where Δtol is the amount of toluene oxidized by OH, F_{pt} is ratio of the particle-phase concentration of the tracer to its total concentration (sum of gas and particle), and F_{Pi} is the ratio of the particle-phase concentration of the volatility bin P_i to its total concentration (sum of gas and particle). F_{pt} and F_{Pi} can be calculated assuming equilibrium partitioning:

$$F_p = \left(1 + \frac{1}{k_{om} \times C_{OA}}\right)^{-1} = \left(1 + \frac{C_i^*}{C_{OA}}\right)^{-1} \quad (10)$$

where k_{om} is the partitioning coefficient of the tracer calculated by the equation described in Zhao et al.(2013)[62] and C_i* is the saturation concentration of the volatility bin P_i, and C_{OA} is the total concentration of SOA formed. Substituting the measurements of f_{SOA} and C_{OA} in Kleindienst et al. (2007) yields the value of α, which is found to be a linear function of the total SOA concentrations (SI Figure S9), indicating that the production of tracer depends on the overall OH exposure. Here we use the α value of 0.028 to estimate the toluene derived SOA concentration in the ambient (SOA_{am}):

$$SOA_{am} = \frac{tracer_{pho}}{\alpha} \cdot \sum_{i=1}^{5} \left(\beta_i \cdot \frac{SOA_{am}}{SOA_{am} + C_i^*}\right) \cdot \left(1 + \frac{1}{k_{om} \times SOA_{am}}\right) \quad (11)$$

where $tracer_{pho}$ is the measured concentrations of the tracer produced from toluene photochemistry, see calculation details given in the SI (Appendix 2 Background Calculation).

The estimated daytime toluene SOA concentrations (Table 1) are 2.3 ± 1.2 μg m^{-3} and 2.3 ± 0.9 μg m^{-3}, respectively, and

Table 1. Daytime Concentrations of the Measured Toluene SOA Tracer and Estimated Toluene SOA Using Updated Tracer-Based Method

site	daytime (month/day)	2,3-dihydroxy-4-oxopentanoic acid(ng m^{-3})	toluene SOA (μg m^{-3})
XH	8/4	5.6	4.3
	8/5	1.7	2.3
	8/6	0.9	1.7
	8/7	0.3	1.0
QP	8/4	3.9	3.6
	8/5	2.5	2.8
	8/6	0.8	1.6
	8/7	0.5	1.3

explain 30.7% and 34.3%, respectively, of the total SOA at Site XH and QP. The fraction of the tracer DHOPA in the particle phase ($f_{SOA,am}$= 0.00063 ± 0.00028, 0.00029−0.00112) is ~6 times lower than those derived from chamber measurements (0.0040 ± 0.0013), implying that results from chamber experiments with high aerosol mass loadings that favor the gas-particle conversion of semivolatile oxidation products may not be adequately representative of the SOA formation processes in the ambient air. The traditional tracer-based method that assumes a constant f_{SOA} factor likely yields a lower limit of the estimated toluene SOA under atmospheric relevant conditions.

3.3. Comparison of the Estimated Toluene SOA by the Two Methods. A comparison of the estimated toluene SOA concentration by the parametrization method with the tracer-based method is given in Figure 2. Uncertainties

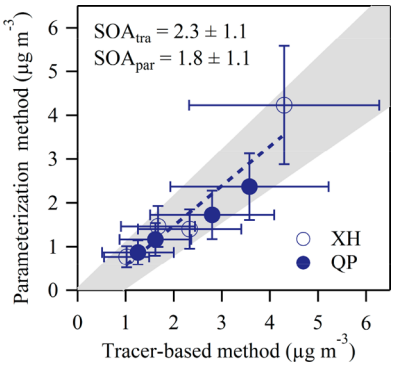

Figure 2. Estimated toluene SOA mass by the parametrization method (SOA_{par}) vs the tracer-based method (SOA_{tra}).

associated with the estimates, that is, 46.5% and 32.5%, respectively, are described in detail in the SI. A positive correlation (r^2 = 0.86) is observed between the two methods with a slope of 0.91, and the tracer-based estimates are higher by 32.8% compared with those derived from the parametrization method. Such an agreement between two independent approaches provides further field evidence for the recently discovered (semi)-solid state of toluene SOA.[61,63] For the parametrization method, the vapor wall loss correction factor was derived by treating the gas-particle partitioning as a kinetically limited process, that is, the time scale for surface accommodation and bulk-phase diffusion is slow, leading to intensive loss of SOA-formation vapors on the wall. It is worth noting, however, that equilibrium portioning is assumed when estimating the SOA production from all other VOCs, which likely leads to an under-correction of the vapor wall loss impact. As a result, the estimated contribution of toluene SOA to the overall SOA mass represents an upper bound compared with historical data. As with the tracer-based method, chamber derived toluene SOA was represented by the recent VBS parametrizations, where the molar fraction of low volatility products (C^* = 0 μg m^{-3}) is a major particle-phase component, leading to the (semi)-solid state of the SOA mixture. Such research suggests the need to improve the SOA prediction capability by current chemical transport models with recent laboratory advances.

■ ASSOCIATED CONTENT

Supporting Information

The Supporting Information is available free of charge on the ACS Publications website at DOI: 10.1021/acs.est.9b00651.

Additional details provided in two appendixes, 10 figures, and four tables (PDF)

■ AUTHOR INFORMATION

Corresponding Authors

*(H.W.) Phone: 86-021-64085119; fax: 86-021-64085119; e-mail: wanghl@saes.sh.cn.
*(X.L.) E-mail: lixiang@fudan.edu.cn.

DOI: 10.1021/acs.est.9b00651
Environ. Sci. Technol. 2019, 53, 8664−8671

ORCID
Hongli Wang: 0000-0003-0655-3389
Xuan Zhang: 0000-0003-1548-8021
Xiang Li: 0000-0002-0434-3057
Li Li: 0000-0001-5575-0894

Notes
The authors declare no competing financial interest.

■ ACKNOWLEDGMENTS

This work was supported by the National Natural Science Foundation of China (No. 21607104) and the Shanghai Science and Technology Commission of Shanghai Municipality (18QA1403600). The National Center for Atmospheric Research (NCAR) is operated by the University Corporation for Atmospheric Research (UCAR), under the sponsorship of the National Science Foundation (NSF) in United States. Thanks to Tadeusz E. Kleindienst from U.S. Environmental Protection Agency (EPA), Dongmin Luo from California Air Resources Board, Neil M. Donahue from Carnegie Mellon University, and Penglin Ye from Aerodyne Research Inc., whose useful conversations improved this manuscript.

■ REFERENCES

(1) Xu, L.; Guo, H.; Boyd, C. M.; Klein, M.; Bougiatioti, A.; Cerully, K. M.; Hite, J. R.; Isaacman-VanWertz, G.; Kreisberg, N. M.; Knote, C.; Olson, K.; Koss, A.; Goldstein, A. H.; Hering, S. V.; de Gouw, J.; Baumann, K.; Lee, S.-H.; Nenes, A.; Weber, R. J.; Ng, N. L. Effects of anthropogenic emissions on aerosol formation from isoprene and monoterpenes in the southeastern United States. *Proc. Natl. Acad. Sci. U. S. A.* **2015**, *112* (32), E4509−E4509.

(2) Spracklen, D. V.; Jimenez, J. L.; Carslaw, K. S.; Worsnop, D. R.; Evans, M. J.; Mann, G. W.; Zhang, Q.; Canagaratna, M. R.; Allan, J.; Coe, H.; McFiggans, G.; Rap, A.; Forster, P. Aerosol mass spectrometer constraint on the global secondary organic aerosol budget. *Atmos. Chem. Phys.* **2011**, *11* (23), 12109−12136.

(3) Kanakidou, M.; Seinfeld, J. H.; Pandis, S. N.; Barnes, I.; Dentener, F. J.; Facchini, M. C.; Van Dingenen, R.; Ervens, B.; Nenes, A.; Nielsen, C. J.; Swietlicki, E.; Putaud, J. P.; Balkanski, Y.; Fuzzi, S.; Horth, J.; Moortgat, G. K.; Winterhalter, R.; Myhre, C. E. L.; Tsigaridis, K.; Vignati, E.; Stephanou, E. G.; Wilson, J. Organic aerosol and global climate modelling: a review. *Atmos. Chem. Phys.* **2005**, *5*, 1053−1123.

(4) Ding, X.; He, Q.; Shen, R.; Yu, Q.; Wang, X. Spatial distributions of secondary organic aerosols from isoprene, monoterpenes, beta-caryophyllene, and aromatics over China during summer. *J. Geophys. Res.-Atmos.* **2014**, *119* (20), 11877−11891.

(5) Ding, X.; Wang, X.; Gao, B.; Fu, X.; He, Q.; Zhao, X.; Yu, J.; Zheng, M. Tracer-based estimation of secondary organic carbon in the Pearl River Delta, south China. *J. Geophys. Res., Atmos.* **2012**, *117*.n/a

(6) Guo, S.; Hu, M.; Guo, Q.; Zhang, X.; Zheng, M.; Zheng, J.; Chang, C. C.; Schauer, J. J.; Zhang, R. Primary sources and secondary formation of organic aerosols in Beijing, China. *Environ. Sci. Technol.* **2012**, *46* (18), 9846−9853.

(7) de Gouw, J. A.; Brock, C. A.; Atlas, E. L.; Bates, T. S.; Fehsenfeld, F. C.; Goldan, P. D.; Holloway, J. S.; Kuster, W. C.; Lerner, B. M.; Matthew, B. M.; Middlebrook, A. M.; Onasch, T. B.; Peltier, R. E.; Quinn, P. K.; Senff, C. J.; Stohl, A.; Sullivan, A. P.; Trainer, M.; Warneke, C.; Weber, R. J.; Williams, E. J. Sources of particulate matter in the northeastern United States in summer: 1. Direct emissions and secondary formation of organic matter in urban plumes. *J. Geophys. Res.* **2008**, *113* (D8), D08301.

(8) Yuan, B.; Hu, W. W.; Shao, M.; Wang, M.; Chen, W. T.; Lu, S. H.; Zeng, L. M.; Hu, M. VOC emissions, evolutions and contributions to SOA formation at a receptor site in eastern China. *Atmos. Chem. Phys.* **2013**, *13* (17), 8815−8832.

(9) Fu, P.; Aggarwal, S. G.; Chen, J.; Li, J.; Sun, Y.; Wang, Z.; Chen, H.; Liao, H.; Ding, A.; Umarji, G. S.; Patil, R. S.; Chen, Q.; Kawamura, K. Molecular markers of secondary organic aerosol in Mumbai, India. *Environ. Sci. Technol.* **2016**, *50* (9), 4659−4667.

(10) Ait-Helal, W.; Borbon, A.; Sauvage, S.; de Gouw, J. A.; Colomb, A.; Gros, V.; Freutel, F.; Crippa, M.; Afif, C.; Baltensperger, U.; Beekmann, M.; Doussin, J. F.; Durand-Jolibois, R.; Fronval, I.; Grand, N.; Leonardis, T.; Lopez, M.; Michoud, V.; Miet, K.; Perrier, S.; Prevot, A. S. H.; Schneider, J.; Siour, G.; Zapf, P.; Locoge, N. Volatile and intermediate volatility organic compounds in suburban Paris: variability, origin and importance for SOA formation. *Atmos. Chem. Phys.* **2014**, *14* (19), 10439−10464.

(11) Tang, R.; Wu, Z.; Li, X.; Wang, Y.; Shang, D.; Xiao, Y.; Li, M.; Zeng, L.; Wu, Z.; Hallquist, M.; Hu, M.; Guo, S. Primary and secondary organic aerosols in summer 2016 in Beijing. *Atmos. Chem. Phys.* **2018**, *18* (6), 4055−4068.

(12) Kleindienst, T. E.; Jaoui, M.; Lewandowski, M.; Offenberg, J. H.; Lewis, C. W.; Bhave, P. V.; Edney, E. O. Estimates of the contributions of biogenic and anthropogenic hydrocarbons to secondary organic aerosol at a southeastern US location. *Atmos. Environ.* **2007**, *41* (37), 8288−8300.

(13) Hu, D.; Bian, Q.; Li, T. W. Y.; Lau, A. K. H.; Yu, J. Z. Contributions of isoprene, monoterpenes, beta-caryophyllene, and toluene to secondary organic aerosols in Hong Kong during the summer of 2006. *J. Geophys. Res.* **2008**, *113*. DOI: 10.1029/2008JD010437

(14) Feng, J.; Li, M.; Zhang, P.; Gong, S.; Zhong, M.; Wu, M.; Zheng, M.; Chen, C.; Wang, H.; Lou, S. Investigation of the sources and seasonal variations of secondary organic aerosols in $PM_{2.5}$ in Shanghai with organic tracers. *Atmos. Environ.* **2013**, *79*, 614−622.

(15) Al-Naiema, I. M.; Yoon, S.; Wang, Y.-Q.; Zhang, Y.-X.; Sheesley, R. J.; Stone, E. A. Source apportionment of fine particulate matter organic carbon in Shenzhen, China by chemical mass balance and radiocarbon methods. *Environ. Pollut.* **2018**, *240*, 34−43.

(16) Volkamer, R.; Jimenez, J. L.; San Martini, F.; Dzepina, K.; Zhang, Q.; Salcedo, D.; Molina, L. T.; Worsnop, D. R.; Molina, M. J. Secondary organic aerosol formation from anthropogenic air pollution: Rapid and higher than expected. *Geophys. Res. Lett.* **2006**, *33* (17), 254−269.

(17) Heald, C. L.; Jacob, D. J.; Turquety, S.; Hudman, R. C.; Weber, R. J.; Sullivan, A. P.; Peltier, R. E.; Atlas, E. L.; de Gouw, J. A.; Warneke, C.; Holloway, J. S.; Neuman, J. A.; Flocke, F. M.; Seinfeld, J. H. Concentrations and sources of organic carbon aerosols in the free troposphere over North America. *J. Geophys. Res.-Atmos.* **2006**, *111* (D23), 23−47.

(18) Heald, C. L.; Jacob, D. J.; Park, R. J.; Russell, L. M.; Huebert, B. J.; Seinfeld, J. H.; Liao, H.; Weber, R. J. A large organic aerosol source in the free troposphere missing from current models. *Geophys. Res. Lett.* **2005**, *32* (18), L18809.

(19) Tsigaridis, K.; Kanakidou, M. Global modelling of secondary organic aerosol in the troposphere: a sensitivity analysis. *Atmos. Chem. Phys.* **2003**, *3*, 1849−1869.

(20) Zhang, X.; Seinfeld, J. H. A functional group oxidation model (FGOM) for SOA formation and aging. *Atmos. Chem. Phys.* **2013**, *13* (12), 5907−5926.

(21) Ensberg, J. J.; Hayes, P. L.; Jimenez, J. L.; Gilman, J. B.; Kuster, W. C.; de Gouw, J. A.; Holloway, J. S.; Gordon, T. D.; Jathar, S.; Robinson, A. L.; Seinfeld, J. H. Emission factor ratios, SOA mass yields, and the impact of vehicular emissions on SOA formation. *Atmos. Chem. Phys.* **2014**, *14* (5), 2383−2397.

(22) Zhang, X.; Cappa, C. D.; Jathar, S. H.; McVay, R. C.; Ensberg, J. J.; Kleeman, M. J.; Seinfeld, J. H. Influence of vapor wall loss in laboratory chambers on yields of secondary organic aerosol. *Proc. Natl. Acad. Sci. U. S. A.* **2014**, *111* (16), 5802−5807.

(23) Fontes, T.; Li, P.; Barros, N.; Zhao, P. Trends of PM2.5 concentrations in China: A long term approach. *J. Environ. Manage.* **2017**, *196*, 719−732.

(24) Huang, R.-J.; Zhang, Y.; Bozzetti, C.; Ho, K.-F.; Cao, J.-J.; Han, Y.; Daellenbach, K. R.; Slowik, J. G.; Platt, S. M.; Canonaco, F.;

DOI: 10.1021/acs.est.9b00651
Environ. Sci. Technol. 2019, 53, 8664−8671

Zotter, P.; Wolf, R.; Pieber, S. M.; Bruns, E. A.; Crippa, M.; Ciarelli, G.; Piazzalunga, A.; Schwikowski, M.; Abbaszade, G.; Schnelle-Kreis, J.; Zimmermann, R.; An, Z.; Szidat, S.; Baltensperger, U.; El Haddad, I.; Prevot, A. S. H. High secondary aerosol contribution to particulate pollution during haze events in China. *Nature* **2014**, *514* (7521), 218−222.

(25) Yao, L.; Wang, D.; Fu, Q.; Qiao, L.; Wang, H.; Li, L.; Sun, W.; Li, Q.; Wang, L.; Yang, X.; Zhao, Z.; Kan, H.; Xian, A.; Wang, G.; Xiao, H.; Chen, J. The effects of firework regulation on air quality and public health during the Chinese Spring Festival from 2013 to 2017 in a Chinese megacity. *Environ. Int.* **2019**, *126*, 96−106.

(26) Xu, J.; Wang, Q.; Deng, C.; McNeill, V. F.; Fankhauser, A.; Wang, F.; Zheng, X.; Shen, J.; Huang, K.; Zhuang, G. Insights into the characteristics and sources of primary and secondary organic carbon: High time resolution observation in urban Shanghai. *Environ. Pollut.* **2018**, *233*, 1177−1187.

(27) Wei, X.-Y.; Liu, M.; Yang, J.; Du, W.-N.; Sun, X.; Huang, Y.-P.; Zhang, X.; Khalil, S. K.; Luo, D.-M.; Zhou, Y.-D. Characterization of PM2.5-bound PAHs and carbonaceous aerosols during three-month severe haze episode in Shanghai, China: Chemical composition, source apportionment and long-range transportation. *Atmos. Environ.* **2019**, *203*, 1−9.

(28) Zhang, C.; Lu, X.; Zhai, J.; Chen, H.; Yang, X.; Zhang, Q.; Zhao, Q.; Fu, Q.; Sha, F.; Jin, J. Insights into the formation of secondary organic carbon in the summertime in urban Shanghai. *J. Environ. Sci.* **2018**, *72*, 118−132.

(29) Ding, X. X.; Kong, L. D.; Du, C. T.; Zhanzakova, A.; Fu, H. B.; Tang, X. F.; Wang, L.; Yang, X.; Chen, J. M.; Cheng, T. T. Characteristics of size-resolved atmospheric inorganic and carbonaceous aerosols in urban Shanghai. *Atmos. Environ.* **2017**, *167*, 625−641.

(30) Gao, W.; Tie, X.; Xu, J.; Huang, R.; Mao, X.; Zhou, G.; Chang, L. Long-term trend of O3 in a mega City (Shanghai), China: Characteristics, causes, and interactions with precursors. *Sci. Total Environ.* **2017**, *603*−*604*, 425−433.

(31) Cheng, Y.; He, K.; Duan, F.; Du, Z.; Zheng, M.; Ma, Y. Ambient organic carbon to elemental carbon ratios: Influence of the thermal-optical temperature protocol and implications. *Sci. Total Environ.* **2014**, *468*, 1103−1111.

(32) Lonati, G.; Giugliano, M.; Butelli, P.; Romele, L.; Tardivo, R. Major chemical components of $PM_{2.5}$ in Milan (Italy). *Atmos. Environ.* **2005**, *39* (10), 1925−1934.

(33) Zeng, T.; Wang, Y. Nationwide summer peaks of OC/EC ratios in the contiguous United States. *Atmos. Environ.* **2011**, *45* (3), 578−586.

(34) Xing, L.; Fu, T. M.; Cao, J. J.; Lee, S. C.; Wang, G. H.; Ho, K. F.; Cheng, M. C.; You, C. F.; Wang, T. J. Seasonal and spatial variability of the OM/OC mass ratios and high regional correlation between oxalic acid and zinc in Chinese urban organic aerosols. *Atmos. Chem. Phys.* **2013**, *13* (8), 4307−4318.

(35) Ram, K.; Sarin, M. M.; Hegde, P. Atmospheric abundances of primary and secondary carbonaceous species at two high-altitude sites in India: Sources and temporal variability. *Atmos. Environ.* **2008**, *42* (28), 6785−6796.

(36) Zhang, Y.; Jia, Y.; Li, M.; Hou, L. A. Characterization of carbonaceous species in $PM_{2.5}$ in Xi'an during spring. *Environ. Forensics* **2018**, *19* (2), 150−154.

(37) Wang, Z.; Wang, T.; Guo, J.; Gao, R.; Xue, L.; Zhang, J.; Zhou, Y.; Zhou, X.; Zhang, Q.; Wang, W. Formation of secondary organic carbon and cloud impact on carbonaceous aerosols at Mount Tai, North China. *Atmos. Environ.* **2012**, *46*, 516−527.

(38) de Gouw, J. A.; Middlebrook, A. M.; Warneke, C.; Goldan, P. D.; Kuster, W. C.; Roberts, J. M.; Fehsenfeld, F. C.; Worsnop, D. R.; Canagaratna, M. R.; Pszenny, A. A. P.; Keene, W. C.; Marchewka, M.; Bertman, S. B.; Bates, T. S. Budget of organic carbon in a polluted atmosphere: Results from the New England Air Quality Study in 2002. *J. Geophys. Res., Atmos.* **2005**, *110*, (D16).

(39) Warneke, C.; McKeen, S. A.; de Gouw, J. A.; Goldan, P. D.; Kuster, W. C.; Holloway, J. S.; Williams, E. J.; Lerner, B. M.; Parrish, D. D.; Trainer, M.; Fehsenfeld, F. C.; Kato, S.; Atlas, E. L.; Baker, A.; Blake, D. R. Determination of urban volatile organic compound emission ratios and comparison with an emissions database. *J. Geophys. Res., Atmos.* 2007, *112*, (D10).

(40) McDonald, B. C.; de Gouw, J. A.; Gilman, J. B.; Jathar, S. H.; Akherati, A.; Cappa, C. D.; Jimenez, J. L.; Lee-Taylor, J.; Hayes, P. L.; McKeen, S. A.; Cui, Y. Y.; Kim, S.-W.; Gentner, D. R.; Isaacman-VanWertz, G.; Goldstein, A. H.; Harley, R. A.; Frost, G. J.; Roberts, J. M.; Ryerson, T. B.; Trainer, M. Volatile chemical products emerging as largest petrochemical source of urban organic emissions. *Science* **2018**, 359 (6377), 760−764.

(41) Roberts, J. M.; Fehsenfeld, F. C.; Liu, S. C.; Bollinger, M. J.; Hahn, C.; Albritton, D. L.; Sievers, R. E. Measurements of aromatic hydrocarbon ratios and NOx concentrations in the rural troposphere-observation of air-mass photochemical aging and NOx removal. *Atmos. Environ.* **1984**, *18* (11), 2421−2432.

(42) Atkinson, R. Gas-phase tropospheric chemistry of organic compounds - a review. *Atmos. Environ., Part A* **1990**, *24* (1), 1−41.

(43) Nelson, P. F.; Quigley, S. M. The meta, para-xylenes-ethylbenzene ratio - a technique for estimating hydrocarbon age in ambient atmospheres. *Atmos. Environ.* **1983**, *17* (3), 659−662.

(44) Vardoulakis, S.; Solazzo, E.; Lumbreras, J. Intra-urban and street scale variability of BTEX, NO2 and O3 in Birmingham, UK: Implications for exposure assessment. *Atmos. Environ.* **2011**, *45* (29), 5069−5078.

(45) de Gouw, J. A.; Gilman, J. B.; Kim, S. W.; Lerner, B. M.; Isaacman-VanWertz, G.; McDonald, B. C.; Warneke, C.; Kuster, W. C.; Lefer, B. L.; Griffith, S. M.; Dusanter, S.; Stevens, P. S.; Stutz, J. Chemistry of Volatile Organic Compounds in the Los Angeles basin: Nighttime Removal of Alkenes and Determination of Emission Ratios. *J. Geophys. Res.-Atmos.* **2017**, *122* (21), 11843−11861.

(46) de Gouw, J. A.; Gilman, J. B.; Kim, S. W.; Alvarez, S. L.; Dusanter, S.; Graus, M.; Griffith, S. M.; Isaacman-VanWertz, G.; Kuster, W. C.; Lefer, B. L.; Lerner, B. M.; McDonald, B. C.; Rappengluck, B.; Roberts, J. M.; Stevens, P. S.; Stutz, J.; Thalman, R.; Veres, P. R.; Volkamer, R.; Warneke, C.; Washenfelder, R. A.; Young, C. J. Chemistry of Volatile Organic Compounds in the Los Angeles Basin: Formation of Oxygenated Compounds and Determination of Emission Ratios. *J. Geophys. Res.-Atmos.* **2018**, *123* (4), 2298−2319.

(47) Borbon, A.; Gilman, J. B.; Kuster, W. C.; Grand, N.; Chevaillier, S.; Colomb, A.; Dolgorouky, C.; Gros, V.; Lopez, M.; Sarda-Esteve, R.; Holloway, J.; Stutz, J.; Petetin, H.; McKeen, S.; Beekmann, M.; Warneke, C.; Parrish, D. D.; de Gouw, J. A. Emission ratios of anthropogenic volatile organic compounds in northern mid-latitude megacities: Observations versus emission inventories in Los Angeles and Paris. *J. Geophys. Res.-Atmos.* **2013**, *118* (4), 2041−2057.

(48) Yuan, B.; Shao, M.; de Gouw, J.; Parrish, D. D.; Lu, S. H.; Wang, M.; Zeng, L. M.; Zhang, Q.; Song, Y.; Zhang, J. B.; Hu, M. Volatile organic compounds (VOCs) in urban air: How chemistry affects the interpretation of positive matrix factorization (PMF) analysis. *J. Geophys. Res.-Atmos.* **2012**, *117*.n/a

(49) Zhu, Y.; Yang, L.; Kawamura, K.; Chen, J.; Ono, K.; Wang, X.; Xue, L.; Wang, W. Contributions and source identification of biogenic and anthropogenic hydrocarbons to secondary organic aerosols at Mt. Tai in 2014. *Environ. Pollut.* **2017**, *220* (Pt B), 863−872.

(50) Draxier, R. R.; Hess, G. D. An overview of the HYSPLIT_4 modelling system for trajectories, dispersion and deposition. *Aust. Meteorol. Mag.* **1998**, *47* (4), 295−308.

(51) Ji, D.; Zhang, J.; He, J.; Wang, X.; Pang, B.; Liu, Z.; Wang, L.; Wang, Y. Characteristics of atmospheric organic and elemental carbon aerosols in urban Beijing, China. *Atmos. Environ.* **2016**, *125*, 293−306.

(52) Yuan, B.; Shao, M.; Lu, S.; Wang, B. Source profiles of volatile organic compounds associated with solvent use in Beijing, China. *Atmos. Environ.* **2010**, *44* (15), 1919−1926.

(53) Deng, Y. Y.; Li, J.; Li, Y. Q.; Wu, R. R.; Xie, S. D. Characteristics of ambient VOCs at the Shuangliu site in Chengdu, China, during summer and autumn. *Huanjing Kexue* **2018**, *39* (12), 5323−5333.

DOI: 10.1021/acs.est.9b00651
Environ. Sci. Technol. 2019, 53, 8664−8671

(54) Cheng, J. H.; Hsieh, M. J.; Chen, K. S. Characteristics and Source Apportionment of Ambient Volatile Organic Compounds in a Science Park in Central Taiwan. *Aerosol Air Qual. Res.* **2016**, *16* (1), 221−229.
(55) Li, L.; Li, H.; Wang, X. Z.; Zhang, X. M.; Wen, C. Pollution characteristics and health risk assessment of atmospheric VOCs in the downtown area of Guangzhou, China. *Huanjing Kexue* **2013**, *34* (12), 4558−4564.
(56) Atkinson, R.; Arey, J. Atmospheric degradation of volatile organic compounds. *Chem. Rev.* **2003**, *103* (12), 4605−4638.
(57) Lewandowski, M.; Jaoui, M.; Offenberg, J. H.; Kleindienst, T. E.; Edney, E. O.; Sheesley, R. J.; Schauer, J. J. Primary and secondary contributions to ambient PM in the midwestern United States. *Environ. Sci. Technol.* **2008**, *42* (9), 3303−3309.
(58) Al-Naiema, I. M.; Stone, E. A. Evaluation of anthropogenic secondary organic aerosol tracers from aromatic hydrocarbons. *Atmos. Chem. Phys.* **2017**, *17* (3), 2053−2065.
(59) Stone, E. A.; Zhou, J.; Snyder, D. C.; Rutter, A. P.; Mieritz, M.; Schauer, J. J. A comparison of summertime secondary organic aerosol source contributions at contrasting urban locations. *Environ. Sci. Technol.* **2009**, *43* (10), 3448−3454.
(60) Stone, E. A.; Hedman, C. J.; Zhou, J. B.; Mieritz, M.; Schauer, J. J. Insights into the nature of secondary organic aerosol in Mexico City during the MILAGRO experiment 2006. *Atmos. Environ.* **2010**, *44* (3), 312−319.
(61) Liu, P.; Li, Y. J.; Wang, Y.; Gilles, M. K.; Zaveri, R. A.; Bertram, A. K.; Martin, S. T. Lability of secondary organic particulate matter. *Proc. Natl. Acad. Sci. U. S. A.* **2016**, *113* (45), 12643−12648.
(62) Zhao, Y.; Kreisberg, N. M.; Worton, D. R.; Isaacman, G.; Weber, R. J.; Liu, S.; Day, D. A.; Russell, L. M.; Markovic, M. Z.; VandenBoer, T. C.; Murphy, J. G.; Hering, S. V.; Goldstein, A. H. Insights into secondary organic aerosol formation mechanisms from measured gas/particle partitioning of specific organic tracer compounds. *Environ. Sci. Technol.* **2013**, *47* (8), 3781−7.
(63) Ye, Q.; Robinson, E. S.; Ding, X.; Ye, P.; Sullivan, R. C.; Donahue, N. M. Mixing of secondary organic aerosols versus relative humidity. *Proc. Natl. Acad. Sci. U. S. A.* **2016**, *113* (45), 12649−12654.

DOI: 10.1021/acs.est.9b00651
Environ. Sci. Technol. 2019, 53, 8664−8671